JOURNAL OF COMPUTATIONAL PHYSICS 101, 330–333 (1992)

Rapid Determination of a Straight Magnetic Coordinate System for Stellarator Configurations*

D. K. LEE AND S. P. HIRSHMAN

Oak Ridge National Laboratory, Oak Ridge, Tennessee 37831

Received June 7, 1990; revised November 15, 1990

A flux coordinate representation for the magnetic field is used to derive a system of simultaneous linear equations for accurately computing the rotational transform and the poloidal angle stream function for a given magnetic flux surface in a toroidal stellarator configuration. The procedure is useful for converting an arbitrary flux coordinate system into one for which all magnetic field lines are straight. It is quite general and requires only that the flux surfaces can be represented by double Fourier series of the coordinates R and Z and that values of the cylindrical components of the magnetic field are available on each surface. Numerical results obtained for vacuum configurations of the Advanced Toroidal Facility (ATF) show that the present procedure is more accurate and convenient than previous methods.

1. INTRODUCTION

In toroidal plasma systems, it is often useful or necessary to perform computations in a magnetic flux coordinate system, where the magnetic field lines are straight. An example requiring such a coordinate system is the estimation of magnetic island widths due to field perturbations in a toroidal stellarator system [1, 2]. While coordinate systems in which the field lines are straight are not unique [3, 4], we present a simple numerical method of determining one such specific coordinate system for which the toroidal angle coordinate is simply the cylindrical angle.

It is assumed that a system of three-dimensional (3D), nested flux surfaces exists in an otherwise arbitrary toroidal magnetic configuration. These surfaces can be represented by a double Fourier series of the form

$$R(\rho, \theta, \phi) = \sum_{m,n} R_{mn}(\rho) \cos(m\theta - n\phi), \tag{1}$$

$$Z(\rho, \theta, \phi) = \sum_{m,n} Z_{mn}(\rho) \sin(m\theta - n\phi), \tag{2}$$

where (R, ϕ, Z) are cylindrical coordinates. In these equations, the variable θ is a parametric coordinate representing a poloidal angle, and ρ is a radial coordinate which is a single-valued function of the toroidal flux Φ and satisfies $\mathbf{B} \cdot \nabla \rho = 0$.

The magnetic field $\mathbf{B}$ can be represented in a contravariant vector form as

$$\mathbf{B} = \nabla \Phi \times \nabla \beta, \tag{3}$$

$$\nabla \beta = \nabla \theta^* - \iota(\rho) \nabla \phi, \tag{4}$$

$$\theta^* = \theta + \lambda(\rho, \theta, \phi), \tag{5}$$

where $\lambda(\rho, \theta, \phi)$ is a stream function, which defines a mapping from θ to a new poloidal angle θ^*. Equations (3) and (4) yield

$$B^{\theta^*}/B^{\phi} = \iota(\rho), \tag{6}$$

where $B^{\theta^*} \equiv \mathbf{B} \cdot \nabla \theta^*$ and $B^{\phi} \equiv \mathbf{B} \cdot \nabla \phi$ are the contravariant poloidal and toroidal components of $\mathbf{B}$, respectively, in the (ρ, θ^*, ϕ) coordinate system. Since the equation defining a field line is

$$\frac{d\theta^*}{d\phi} = \frac{B^{\theta^*}}{B^{\phi}}, \tag{7}$$

it follows that, along a field line,

$$\frac{d\theta^*}{d\phi} = \iota(\rho). \tag{8}$$

Thus, field lines are straight in the (ρ, θ^*, ϕ) coordinate system.

A method of evaluating the Fourier representation for the stream function

$$\lambda(\rho, \theta, \phi) = \sum_{m,n} \lambda_{mn}(\rho) \sin(m\theta - n\phi) \tag{9}$$

* Research sponsored by the Office of Fusion Energy, U. S. Department of Energy, under Contract DE-AC05-84OR21400 with Martin Marietta Energy Systems, Inc.

0021-9991/92 $5.00

is given in Ref. [5]. However, this method is numerically cumbersome, and a high degree of accuracy is not easy to achieve, since it requires the Jacobian of the transformation from (R, ϕ, Z) to (ρ, θ, ϕ) and the corresponding metric tensor elements, which involve radial derivatives $\partial R/\partial\rho$ and $\partial Z/\partial\rho$. Thus, one must obtain the Fourier representations given by Eqs. (1) and (2) not only for the surface(s) of interest, but also for neighboring surfaces.

The purpose of this paper is to describe an alternative procedure of evaluating $\lambda_{mn}(\rho)$, which relies on a knowledge of cylindrical components of the magnetic field, rather than $\partial R/\partial\rho$ and $\partial Z/\partial\rho$, on the flux surface. Both of these methods require availability of the flux surface representation in the form of Eqs. (1) and (2). Note that the variable θ in this representation is quite general in that it can be any coordinate representing a poloidal angle, although θ used in Ref. [5] is chosen such that the Fourier series given by Eqs. (1) and (2) are most compact and θ used in the numerical examples in the present study (Section 3) is taken to be the ordinary geometric poloidal angle.

2. NEW METHOD

To describe a simpler and potentially more accurate method of determining $\lambda_{mn}(\rho)$, we employ the following expressions for the contravariant components of **B**:

$$B^\theta = \frac{1}{\sqrt{g}}\frac{d\Phi}{d\rho}\left(\iota - \frac{\partial\lambda}{\partial\phi}\right), \tag{10}$$

$$B^\phi = \frac{1}{\sqrt{g}}\frac{d\Phi}{d\rho}\left(1 + \frac{\partial\lambda}{\partial\theta}\right), \tag{11}$$

$$B^R = B^\theta\frac{\partial R}{\partial\theta} + B^\phi\frac{\partial R}{\partial\phi}, \tag{12}$$

$$B^Z = B^\theta\frac{\partial Z}{\partial\theta} + B^\phi\frac{\partial Z}{\partial\phi}. \tag{13}$$

In these equations, it is assumed that not only is the flux surface geometry known from Eqs. (1) and (2), but also the cylindrical components of **B**, (B^R, B^ϕ, B^Z), and the toroidal flux, $\Phi(\rho)$, are known. Thus, it is possible to obtain ι and λ from these equations. The resulting partial differential equation is

$$\frac{B^\theta}{B^\phi} = \frac{\iota - \partial\lambda/\partial\phi}{1 + \partial\lambda/\partial\theta} = \frac{\xi}{g_{\theta\theta}}, \tag{14}$$

where

$$g_{\theta\theta} = \left(\frac{\partial R}{\partial\theta}\right)^2 + \left(\frac{\partial Z}{\partial\theta}\right)^2, \tag{15}$$

$$\xi = \frac{\partial R}{\partial\theta}\left(\frac{B^R}{B^\phi} - \frac{\partial R}{\partial\phi}\right) + \frac{\partial Z}{\partial\theta}\left(\frac{B^Z}{B^\phi} - \frac{\partial Z}{\partial\phi}\right). \tag{16}$$

Note that Eqs. (12) and (13) are redundant in the sense that B^θ/B^ϕ can be obtained from either one of them. The particular form of $B^\theta/B^\phi = \xi/g_{\theta\theta}$ given in Eq. (14) is especially useful, since it avoids potential numerical problems near extrema where $\partial R/\partial\theta = 0$ or $\partial Z/\partial\theta = 0$. This is apparent since $g_{\theta\theta} \neq 0$ (arc length derivative), and hence no zeroes occur in the denominator of the expression for B^θ/B^ϕ. In Eq. (14), the quantities ξ and $g_{\theta\theta}$ are assumed to be known.

Substitution of the Fourier series for $\partial\lambda/\partial\theta$ and $\partial\lambda/\partial\phi$ derived from Eq. (9) into Eq. (14) yields

$$\iota(\rho)\, g_{\theta\theta} + \sum_{m,n} (\lambda_{mn}(\rho)(n g_{\theta\theta} - m\xi)\cos(m\theta - n\phi) = \xi. \tag{17}$$

To determine the unknown variables ι and λ_{mn}, we multiply both sides of Eq. (17) by $\cos(\mu\theta - \nu\phi)$ and average over the domain $0 \leqslant \theta \leqslant 2\pi$ and $0 \leqslant \phi \leqslant 2\pi$. This yields a system of linear simultaneous equations for ι and λ_{mn},

$$a^{\mu\nu}\iota(\rho) + \sum_{m,n} b^{\mu\nu}_{mn}\lambda_{mn}(\rho) = c^{\mu\nu}, \tag{18}$$

where

$$a^{\mu\nu} = \langle g_{\theta\theta}\cos(\mu\theta - \nu\phi)\rangle, \tag{19}$$

$$b^{\mu\nu}_{mn} = \langle (n g_{\theta\theta} - m\xi)\cos(m\theta - n\phi)\cos(\mu\theta - \nu\phi)\rangle, \tag{20}$$

$$c^{\mu\nu} = \langle \xi\cos(\mu\theta - \nu\phi)\rangle, \tag{21}$$

$$\langle f(\theta, \phi)\rangle \equiv \frac{1}{(2\pi)^2}\int_0^{2\pi}\int_0^{2\pi} f(\theta, \phi)\, d\theta\, d\phi. \tag{22}$$

The set (μ, ν) is chosen to coincide with (m, n), and includes the $(0, 0)$ term for determining ι. Then, Eq. (17) gives the same number of independent equations as the number of unknowns ι and λ_{mn}, allowing ι and λ_{mn} to be determined uniquely.

3. NUMERICAL TEST RESULTS

To examine the numerical accuracy and utility of the method based on Eq. (18) and to compare them with those of the method described in Ref. [5], we have used both procedures to evaluate $\iota(\rho)$ and $\lambda_{mn}(\rho)$ for the configuration of the Advanced Toroidal Facility (ATF). Here we choose the poloidal variable θ to be the ordinary geometric angle:

$$\theta = \tan^{-1}[(Z - Z_0)/(R - R_0)], \tag{23}$$

where (R_0, Z_0) is the magnetic axis position. The radial coordinate is defined by

$$\rho = (\Phi/\pi B_0)^{1/2}, \tag{24}$$

where Φ is the toroidal magnetic flux and B_0 is the average magnetic field at the axis, $\rho = 0$. Note that our choice of ρ by Eq. (24) closely approximates the average minor radius

TABLE I

Numerical Values of ρ, ι, and $\Delta\theta^*$ for Flux Surfaces near the Rational Surface with $\iota = \frac{1}{2}$

		ι			$\Delta\theta^*$(deg)	
Surface	ρ(cm)	Exact	Eq. (18)	Ref. [5]	Eq. (18)	Ref. [5]
1	18.10	0.52405	0.52395	0.52425	0.0315	0.0158
2	17.81	0.51664	0.51657	0.51682	0.0235	0.0159
3	17.53	0.50929	0.50918	0.50941	0.0295	0.0223
4	17.23	0.50206	0.50199	0.50216	0.0253	0.0310
5	17.15	0.50000	0.49992	0.50010	0.0240	0.0343
6	17.06	0.49797	0.49790	0.49806	0.0221	0.0397
7	16.76	0.49086	0.49077	0.49094	0.0269	0.0460
8	16.47	0.48434	0.48428	0.48441	0.0200	0.0524
9	16.17	0.47779	0.47770	0.47786	0.0266	0.0562

for essentially any toroidal device and not just that of the ATF. Along a field line on the flux surface ρ, we let

$$\theta^*(\phi) = \theta^*(\phi_0) + \iota(\rho)(\phi - \phi_0), \tag{25}$$

$$\theta_a^*(\phi) = \theta(\phi) + \sum_{m,n} \lambda_{mn}(\rho) \sin[m\theta(\phi) - n\phi]. \tag{26}$$

A measure of accuracy of the computed $\lambda_{mn}(\rho)$ is provided by the rms value deviation of $\theta_a^*(\phi)$ from $\theta^*(\phi)$:

$$\Delta\theta^* = \langle [\theta_a^*(\phi) - \theta^*(\phi)]^2 \rangle^{1/2}. \tag{27}$$

Table I lists two sets of numerical results for ι and $\Delta\theta^*$ at nine flux surfaces near the rational surface with $\iota = \frac{1}{2}$; one set was obtained by solving Eq. (18) and the other with the method described in Ref. [5]. The exact values of ι were determined by following field lines at least 1000 turns around the major axis through numerical integration of the field line equations. Values of $\Delta\theta^*$ were calculated by following field lines on the flux surfaces four turns around the major axis. Table II gives similar results evaluated at nine surfaces near the rational surface with $\iota = \frac{1}{3}$. The choice of (m, n) modes included in the sums of Eqs (1), (2), (9), and

TABLE II

Numerical Values of ρ, ι, and $\Delta\theta^*$ for Flux Surfaces near the Rational Surface with $\iota = \frac{1}{3}$

		ι			$\Delta\theta^*$(deg)	
Surface	ρ(cm)	Exact	Eq. (18)	Ref. [5]	Eq. (18)	Ref. [5]
1	8.49	0.34605	0.34598	0.34598	0.0263	0.0479
2	7.86	0.34034	0.34027	0.34050	0.0271	0.0369
3	7.28	0.33559	0.33550	0.33592	0.0279	0.0270
4	7.14	0.33447	0.33438	0.33484	0.0286	0.0261
5	7.00	0.33338	0.33328	0.33377	0.0289	0.0246
6	6.86	0.33230	0.33221	0.33272	0.0291	0.0248
7	6.71	0.33124	0.33115	0.33167	0.0297	0.0258
8	6.03	0.32654	0.32642	0.32693	0.0372	0.0385
9	4.73	0.31902	0.31897	0.31877	0.0418	0.0691

TABLE III

Numerical Values of ι, and $\Delta\theta^*$ Evaluated with the Method of Ref. [5]

			$\iota_{exact} = 0.50000$		$\iota_{exact} = 0.33338$	
Surfaces used	N_{surf}	K	ι	$\Delta\theta^*$(deg)	ι	$\Delta\theta^*$(deg)
1–9	9	4	0.50018	0.0696	0.33336	0.2006
1–9	9	3	0.50017	0.0844	0.33335	0.2345
1–9	9	2	0.50035	0.0317	0.33354	0.1203
2–8	7	3	0.50004	0.1156	0.33343	0.0215
2–8	7	2	0.50028	0.0456	0.33340	0.1965
1–3, 5, 7–9	7	3	0.50019	0.0614	0.33335	0.2417
1–3, 5, 7–9	7	2	0.50035	0.0262	0.33354	0.1226
3–7	5	3	0.49984	0.9206	0.33343	0.0252
3–7	5	2	0.50014	0.0916	0.33342	0.0257
2, 3, 5, 7, 8	5	3	0.50007	0.0358	0.33342	0.0226
2, 3, 5, 7, 8	5	2	0.50029	0.0324	0.33340	0.2003
4–6	3	1	0.49985	0.8711	0.33343	0.0255
3, 5, 7	3	1	0.50005	0.0395	0.33341	0.0261

(26) was based on the requirement $R_{mn}^2(\rho) + Z_{mn}^2(\rho) > 10^{-10}\ \mathrm{m}^2$ for the rational surface of interest ($\iota \approx \frac{1}{2}$ or $\frac{1}{3}$), and the same modes were used for all other surfaces in the vicinity. The number of modes selected in this way is 55 for surfaces in Table I and 57 for surfaces in Table II. As mentioned earlier, the method of Ref. [5] involves the derivatives $dR_{mn}(\rho)/d\rho$ and $dZ_{mn}(\rho)/d\rho$, and therefore we have chosen enough numbers of the flux surfaces near the two rational surfaces to ensure a highest available accuracy at the surfaces of interest (surface 5 in Tables I and II). The radial derivatives were evaluated using least-squares polynomial approximation routines in the NAG Library with $K = 4$, where K is the highest degree of the polynomials. Numerical values of ι and $\Delta\theta^*$ listed in Table III were obtained using the method of Ref. [5] at the two surfaces ($\iota \approx \frac{1}{2}, \frac{1}{3}$) as in Tables I and II, but many different sets of surfaces and different values of K where tried to show that the accuracy of the method of Ref. [5] is sensitive to the approximation scheme used to evaluate the radial derivatives of R and Z. In the Table III entries under "Surfaces used" show the surface numbers (labels) given in Tables I and II for the surfaces with $\iota \approx \frac{1}{2}$ and $\frac{1}{3}$, respectively, and N_{surf} means the total number of surfaces used.

In Fig. 1, poloidal angles $\theta(\phi)$, $\theta^*(\phi)$, and $\theta_a^*(\phi)$ are plotted versus ϕ along a field line on the rational surface with $\iota = \frac{1}{2}$. Numerical values of $\theta_a^*(\phi)$, obtained at 1728 equally spaced points of ϕ, are shown as small dots, but they are so close to the corresponding values of $\theta^*(\phi)$ (the straight line given by Eq. (25)) that the difference between $\theta_a^*(\phi)$ and $\theta^*(\phi)$ can hardly be seen on the scale of the figure. The 55 values of $\lambda_{mn}(\rho)$ determined by solving Eq. (18) were used for $\theta_a^*(\phi)$. Figure 2 shows the difference $\theta_a^*(\phi) - \theta^*(\phi)$ evaluated with the same $\lambda_{mn}(\rho)$ and along the same field line as in the case of Fig. 1.

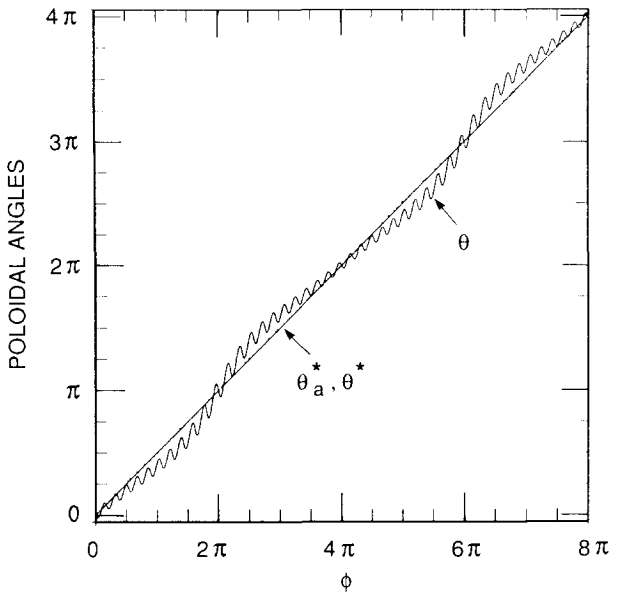

FIG. 1. Poloidal angles θ, θ^* (Eq. (25)), and θ_a^* (Eq. (26)) are shown as functions of ϕ along a field line on the rational flux surface with $\iota = \frac{1}{2}$. The numerical values of θ_a^* (dots) are so close to the corresponding values of θ^* (straight line) that the difference is hard to see on this scale.

We conclude this section with some remarks concerning the numerical procedure used to determine the Fourier representations for the flux surfaces given in Tables I and II, in particular, for the two rational surfaces with $\iota \approx \frac{1}{2}$ and $\frac{1}{3}$. To evaluate Fourier coefficients in Eqs. (1) and (2), we used 240 reasonably uniformly distributed Poincaré puncture points at each of 16 equally spaced toroidal planes in a single field period, $0 \leqslant \phi < 2\pi/N_{fp}$, where $N_{fp} = 12$ is the number of field periods. The coefficients were computed by applying a least-squares fitting method to these 240×16 data points. For a low-order rational surface, obtaining such flux surface points by following a field line presents some numerical difficulties, since the field line closes on itself after m toroidal transits, if $\iota = n/m$. In our model of the ATF, however, we have observed that there are extremely small islands at the location of the surface with $\iota = \frac{1}{2}$. The island formation is completed after 2396 toroidal transits along a field line, and the maximum island widths are no larger than 2 mm. Although the two islands are far apart from each other (no x-points), their poloidal spread is wide enough to generate a complete flux surface, if puncture points from the 12 topologically equivalent (symmetry) toroidal planes are combined (overlaid) to form a single flux surface at a given toroidal angle. The flux surface with $\iota = \frac{1}{3}$, on the other hand, could not be determined in a similar way, since no islands could be found. We chose, therefore, a surface very close to the one with $\iota = \frac{1}{3}$. It took 7152 toroidal transits to complete the surface, which means that the deviation of ι from $\frac{1}{3}$ is $(3 \times 7152)^{-1} = 4.66 \times 10^{-5}$, or $\iota = 0.3333799$. We have not been able to identify the source(s) of islands with $\iota = \frac{1}{2}$.

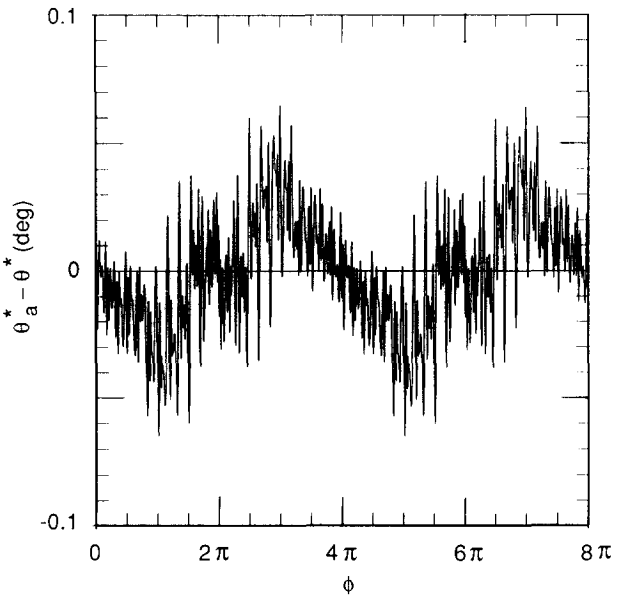

FIG. 2. The error of θ_a^* vs ϕ along the same field line as in Fig. 1. Values of $\lambda_{mn}(\rho)$ determined by solving Eq. (18) were used to evaluate θ_a^*.

4. CONCLUDING REMARKS

Two different methods of evaluating $\lambda_{mn}(\rho)$ have been compared: one is based on Eq. (18), and the other is described in Ref. [5]. In general, the former is more accurate and more convenient than the latter, if the magnetic field is known in addition to the flux surface geometry. On the other hand, if the magnetic field is not known on each surface, the present method fails, and it is necessary to obtain Fourier representations of many surfaces to evaluate radial derivatives of R and Z for use in the method of Ref. [5]. Our numerical results, obtained for the ATF configuration, indicate that both methods are fairly straightforward to apply and no serious difficulties are expected to arise in the numerical procedure. Although our study is concerned with three-dimensional flux coordinate systems, the method is somewhat similar to a two-dimensional analysis of mapping from a rectangular to a harmonic representation developed by Schneider and Bateman [6].

REFERENCES

1. A. I. Morozov and L. S. Solov'ev, *Reviews of Plasma Physics*, edited by M. A. Leontovich (Consultants Bureau, New York, 1966), Vol. 2, p. 1.
2. D. K. Lee, J. H. Harris, and G. S. Lee, *Nucl. Fusion* **30**, 2177 (1990).
3. G. Kuo-Petravic, A. H. Boozer, J. A. Rome, and R. H. Fowler, *J. Comput. Phys.* **51**, 261 (1983).
4. S. Hamada, *Nucl. Fusion* **1**, 23 (1962).
5. D. K. Lee, J. H. Harris, S. P. Hirshman, and G. H. Neilson, *Nucl. Fusion* **28**, 1351 (1988).
6. W. Schneider and G. Bateman, *J. Comput. Phys.* **71**, 169 (1987).